Journal of Medicinal Chemistry

Article

Cite This: J. Med. Chem. 2017, 60, 9003-9011

pubs.acs.org/jmc

Lipoyl-Homotaurine Derivative (ADM_12) Reverts Oxaliplatin-Induced Neuropathy and Reduces Cancer Cells Malignancy by Inhibiting Carbonic Anhydrase IX (CAIX)

Marco Fragai,[†,‡] Giuseppina Comito,[§] Lorenzo Di Cesare Mannelli,[∥] Roberta Gualdani,[†] Vito Calderone,[†,‡] Alexandra Louka,[‡] Barbara Richichi,[†] Oscar Francesconi,[†] Andrea Angeli,[∥] Alessio Nocentini,[∥] Paola Gratteri,[∥] Paola Chiarugi,[§] Carla Ghelardini, Francesco Tadini-Buoninsegni,[†] Claudiu T. Supuran,[*,∥] and Cristina Nativi[*,†,⊥]

[†]Department of Chemistry, University of Florence, via della Lastruccia 3-13, 50019 Sesto Fiorentino, Italy

[‡]CERM, University of Florence, via L. Sacconi 6, 50019 Sesto Fiorentino, Italy

[§]Department of Experimental and Clinical Biomedical Sciences, University of Florence, V.le Morgagni 50, 50134 Firenze, Italy

[∥]Department NEUROFARBA, University of Florence, V.le Pieraccini 6, 50134 Firenze, Italy

[⊥]FioGen, via L. Sacconi 6, 50019 Sesto Fiorentino, Italy

Supporting Information

ABSTRACT: Oxaliplatin (OXA) is a valuable and largely used cancer drug which induces a serious and intractable neuropathy. The lipoyl-homotaurine derivative (**ADM_12**) reverts in vivo OXA-induced neuropathy, and it is an effective antagonist of the nociceptive sensor channel TRPA1. Unprecedentedly, this safe analgesic showed a synergy with OXA in vitro and proved to inhibit CA IX, a relevant therapeutic target, clearly interfering with pancreatic cancer cells' aggressiveness.

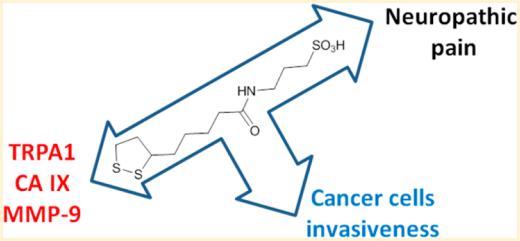

INTRODUCTION

The number of cancer patients is increasing worldwide, and a large majority of them receive antitumoral chemotherapy. The development of new and effective anticancer drugs has extended the survival of tumor-bearing hosts, conceivably raising the proportion of patients having experienced chemotherapy-induced neuropathy (CIN).[1] CIN is considered one of the most disabling and invalidating diseases affecting cancer patients: CIN induces or worsens depression, insomnia, and distress, greatly affecting the quality of life and often becoming the treatment-limiting issue in cancer therapy.[2,3] Therapeutically, CIN is still considered an intractable problem. As a matter of fact, no pharmacological treatments have demonstrated efficacy in the prevention or therapy of CIN. Mixtures of opioids and nonopioids, including vitamins and mineral salts, are generally administrated with scarce or no evidence of efficacy, confirming CIN as the major concern for both cancer patients and oncologists.[4] Manifestations and causes of CIN can vary substantially from drug to drug. A distinct, and probably one of the most difficult to treat, is the neuropathy induced by oxaliplatin (OXA). Mechanical and cold allodynic sensation in hands and feet are the painful effects produced which, surprisingly, may worsen after OXA administration has finished.[2] Thus, the availability of safe and effective analgesic drugs for the treatment of chronic CIN is a task of primary importance as well as an urgent need. Acute and chronic peripheral neuropathies associated with the use of OXA have extensively been reported[5] and related to the remodeling and alteration in the expression of transient receptors potential (TRP) Ca^{2+} channels. In particular, potential thermosensitive transient receptors vanilloid 1 (TRPV1) and ankyrin 1 (TRPA1) are upregulated and hypersensitized, mediating OXA-evoked cold and mechanical allodynia.[6,7] We recently reported about the TRPA1 antagonist **1** (**ADM_09**) (Figure 1),[8] which effectively reverts neuropathic pain evoked by OXA without eliciting the negative side-effects generally observed in neuropathic pain treatment. Preserving the α-lipoic portion, which characterizes **1**, we have also reported a second lipoic-containing TRPA1 antagonist, namely **2** (**ADM_12**) (Figure 1),[9] successfully assayed to treat in vivo another orphan pain, that is, the orofacial pain.[9]

With respect to **1**, **2** presents the lipoic acid portion linked to an homotaurine and is characterized by a terminal sulfonic acid residue.[9] In a recent paper describing the inhibitory activity of a bromophenol sulfonic acid vs human (*h*) carbonic anhydrases (*h*CAs, EC 4.2.1.1) implicated in cancer progression,[10] some of us proved the involvement of the sulfonic acid residue in the binding to the CA IX active site by anchoring to the zinc-coordinated water molecule. Keeping this in mind and capitalizing on data we previously reported for **2**, we reasoned that **2** might be an excellent candidate for both the treatment of

Received: August 22, 2017
Published: October 19, 2017

DOI: 10.1021/acs.jmedchem.7b01237
J. Med. Chem. 2017, 60, 9003−9011

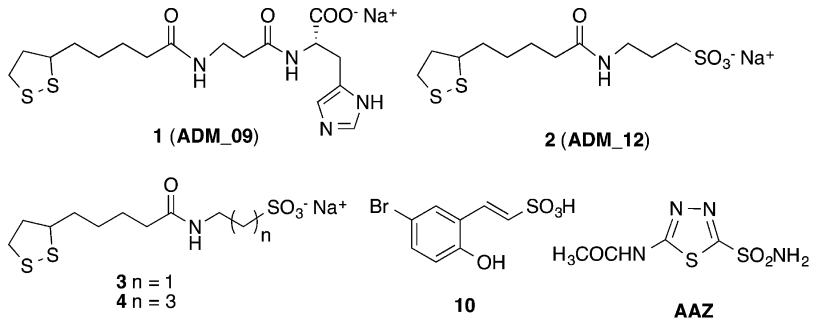

Figure 1. Structures of **1**, **2**, **3**, **4**, **10**, and acetazolamide (AAZ).

Scheme 1. Synthesis of Lipoic-Containing Derivatives 3, 4, and 9

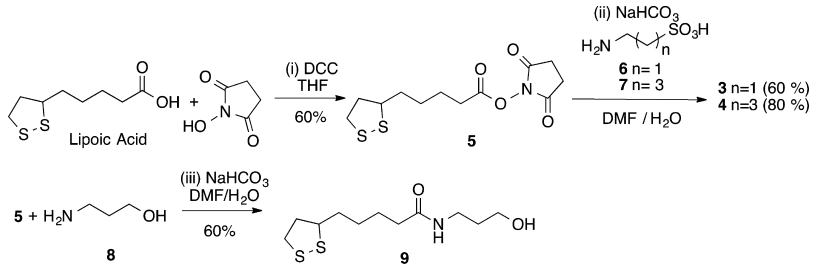

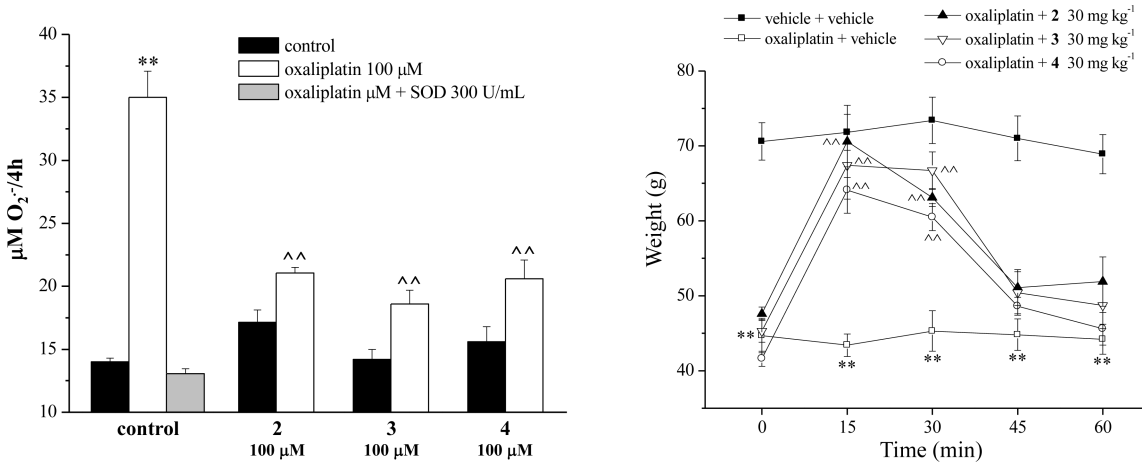

Figure 2. (A) SOD-inhibitable $O_2^{\bullet-}$ levels in astrocyte cell lines. Astrocytes (5 × 105 cells/well, two control wells and two wells pretreated with **2**, **3**, or **4**) were exposed to 100 μM OXA for 4 h. The effect of 100 μM **2** coincubation on SOD-inhibitable superoxide anion $O_2^{\bullet-}$ on levels are depicted. The nonspecific absorbance measured in the presence of SOD was subtracted from the total value. Values are expressed as mean ± SEM of three experiments. $^{**}P < 0.01$ vs control and $^{\wedge\wedge}P < 0.01$ vs OXA treatment. (B) OXA-induced neuropathic pain: antihypersensitive effect of **2** in comparison to **3** and **4**. Rats were daily treated ip with 2.4 mg kg^{-1} OXA (in 0.5% glucose solution). The response to a noxious mechanical stimulus was evaluated on day 21 by the paw-pressure test. Vehicle (1% CMC) or 30 mg kg^{-1} **2**, **3**, or **4** were administered po, and measurements were performed over time. Each value represents the mean ± SEM of 12 rats per group, performed in two different experimental sets. $^{*\wedge}P < 0.01$ vs vehicle + vehicle; $^{\wedge\wedge}P < 0.01$ vs OXA + vehicle.

neuropathic pain induced by OXA and as a new inhibitor of CAs. Hence, we report herein on the investigation of **2** and the corresponding homologues **3** and **4** (Figure 1) in (a) the treatment of OXA-induced neuropathy (OXAIN), (b) binding tests vs CA IX and CA XII, as well as (c) in CA IX-mediated cancer cells motility tests. Unprecedentedly, our data showed the double role of **2** as an analgesic but also as a modulator in cancer cells' invasiveness.

RESULTS

Synthesis. Following the synthetic strategy reported for **2**,[9] its homologous **3** and **4** were obtained in two steps by reacting the commercially available (±) α-lipoic acid with *N*-hydroxysuccinimide in tetrahydrofuran (THF) as solvent and in the presence of dicyclohexylcarbodiimide (DCC) to give the activated lipoic derivative **5** (Scheme 1). The unreacted DCC and the dicyclohexyl urea formed during the reaction were removed by crystallization, and pure **5** was treated with taurine **6** or with the amino sulfonic acid **7** in H_2O/DMF to afford, after purification, **3** (60%) or **4** (80%), respectively. As reported for **3** and **4** (see Scheme 1), the lipoic-containing alcohol **9**, used as control (see below), was obtained by reacting **5** with the amino alcohol **8** (Supporting Information). After purification, **9** was isolated as a yellow waxy solid in 60% yield.

Antioxidative Properties. As widely reported,[11,12] acute and chronic neurotoxicities associated with the use of OXA are

DOI: 10.1021/acs.jmedchem.7b01237
J. Med. Chem. 2017, 60, 9003−9011

Table 1. Viability Cell Test (MTT) Run 24 h after the Treatment with OXA and 2[a]

		OXA 1 μM	OXA 10 μM	OXA 30 μM	OXA 100 μM	OXA 300 μM
control	100 ± 2.2					
2 (100 μM)	81.3 ± 3.1*	74.6 ± 3.2**	78.6 ± 0.8**	71.4 ± 1.1***	67.4 ± 3.6***^	48.1 ± 2.6***^^^

[a]The % of viable cells with respect to the control is reported. **$p < 0.01$ and ***$p < 0.001$ vs control; ^$p < 0.05$ and ^^^$p < 0.01$ vs **2** alone.

related to the oxidative stress caused by this cancer drug. Therefore, the antioxidant profiles of **2**, **3**, and **4** were evaluated. We measured the oxidation in vitro of nitro blue tetrazolium (NBT) after 30 min in the absence and in the presence of an increasing concentration of **2** (Table S2, Supporting Information). The superoxide anion ($O_2^{\bullet-}$) generated by the hypoxanthine−xanthine oxidase system increased the oxidized NBT level from 100 (basal) to about 4000 a.u. In the presence of **2** in the reaction mixture, the oxidation of NBT was inhibited in a concentration-dependent manner, taking effect starting from 10 μM, the highest concentration (1000 μM) allowed to obtain a complete prevention of oxidation. Similar results were observed testing **3** and **4** but, differently from **2**, they were not able to fully prevent the oxidation (Supporting Information). The antioxidative properties were also tested in a cell culture of primary rat cortical astrocytes, a cell type strongly involved in OXA-dependent neuropathy.[13,14] A 4 h long cell treatment with 100 μM OXA induced a significant, SOD-inhibitable, superoxide anion increase as evaluated by the cytochrome C assay (Figure 2A). The coincubation with 100 μM **2** or **3** or **4** inhibited the $O_2^{\bullet-}$ formation by about 75% in comparison to the untreated culture.

Antihyperalgesic Properties. To evaluate the pain-relieving property of the tested compounds, a painful neuropathic condition was reproduced in rats with a repeated treatment with OXA (2.4 mg kg^{-1}, ip, daily). On day 21, the pain threshold was measured by the paw pressure test by applying a noxious mechanical stimulus. Oxaliplatin-treated animals showed (Figure 2B) a decreased threshold reported as a reduced weight tolerated on the paw (44.7 ± 2.3 g in comparison to 70.6 ± 2.5 g of control animals). Compound **2**, acutely administered po (30 mg kg^{-1}), counteracted the OXA-induced hypersensitivity, taking effect 15 min after treatment. A complete reversion of pain lasted up to 75 min. A similar profile was observed for compounds **3** and **4** (Figure 2B) even though a complete reversion of the noxious effect is observed only with **2**.

Synergistic Effect of OXA and 2. The soundness data obtained with **2** in reverting OXAIN in vivo, suggested to investigate a possible synergistic effect of **2** and OXA. The activity profile of **2** against tumor cells was thus evaluated in human colon cancer cell lines HT-29. The incubation with increasing concentrations of **2** (1−300 μM) for 24 h induced a progressive decreasing of cell viability as evaluated by MTT test, reaching 20% of mortality (Table S3, Supporting Information). Moreover, **2** was also analyzed in the presence of the neurotoxic anticancer drug OXA. As shown in Table S4, Supporting Information, OXA in HT-29 cells is active at 30, 100, and 300 μM (24 h). In the presence of **2** (100 μM), OXA activity was not decreased; on the contrary, **2** increased OXA potency, decreasing cell viability starting out at 1 μM, reaching significant differences at 100 and 300 μM (Table 1). The analysis of synergism performed by the Chou−Talalay method revealed a combination index (CI) 0.5 considered as "synergism".

Inhibition of TRPA1 Activated with OXA. As reported,[9] **2** can inhibit TRPA1 methanol- and AITC-evoked current with a low micromolar constant. Thus, using the patch clamp technique, we investigated the effect of **2** on TRPA1 evoked current by OXA. After perfusion of OXA 50 μM, we observed the activation of TRPA1 channel, which is rapidly and completely reverted in the presence of **2**, 30 μM. The corresponding time courses (Figure 3A) and IV curves (Figure S2, Supporting Information) are reported (see Table S1 and Figure S1, Supporting Information, for details about compounds **3** and **4**).

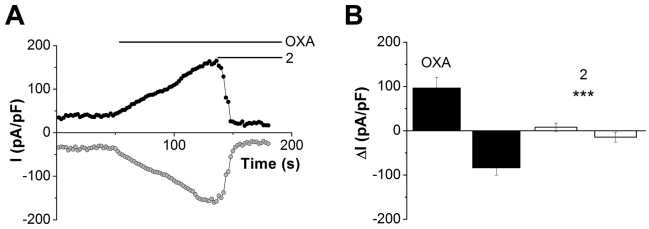

Figure 3. (A) Time course obtained from voltage ramps measured at +50 mV (black circles) and −50 mV (gray circles). OXA (50 μM) and **2** (30 μM) were applied at the time indicated. CHO cells were transfected with wild-type TRPA1 channel. (B) Summarized data of TRPA1 whole-cell currents evoked by OXA (50 μM) and OXA + **2** (30 μM). Each column represents mean ± SEM of $n = 5$ cells. *** $p < 0.0001$ (unpaired Student's t test).

Compound 2 Inhibits Carbonic Anhydrases IX and XII. Carbonic anhydrases (CAs, EC 4.2.1.1) are zinc metalloenzymes that catalyze the hydration of carbonic dioxide, producing bicarbonate and protons.[15,16] CA IX is a transmembrane enzyme upregulated in many cancer types and playing an important role in the acidification of the outer microenvironment under hypoxia, a hallmark of many tumors.[17] The involvement of CA IX to acidification of the tumor environment has been correlated with the acquisition of metastatic phenotypes and is related to a decrease in the success of anticancer drugs.[18] Recently, some of us reported on the nanomolar *h*CA IX and *h*CA XII inhibitor **10** (see Figure 1), presenting a sulfonic acid residue involved in the binding to the CA IX active site by anchoring to the zinc-coordinated water molecule.[10] Of note, currently a sulfonamide CA IX inhibitor completed phase I clinical trials for the treatment of advanced stage solid tumors and is scheduled for phase II trials.[19] Keeping in mind the specific CA inhibition mechanism of **10**, we investigated **2** as a possible ligand for CA IX and CA XII. In fact, even though the properties of **2**, **3**, and **4** as TRPA1 inhibitors or to revert OXAIPN are rather similar, overall, the pharmacological profile of **2** is the most interesting. For this reason, all the following tests have been performed on **2** selected as a lead molecule. We investigated the CA inhibitory activity of **2** by applying the stopped flow carbon dioxide hydrase assay (Supporting Information) in comparison to acetazolamide (AAZ, see Figure 1) as standard CA inhibitor against the tumor-associated isoforms *h*CA IX and XII (Table

DOI: 10.1021/acs.jmedchem.7b01237
J. Med. Chem. 2017, 60, 9003−9011

2; see Table S5, Supporting Information, for inhibition data vs other *h*CAs and Figure S3, Supporting Information, for dose

Table 2. Inhibition Data of Human CA Isoforms *h*CA IX and XII with 2, Compound 10, and the Standard Sulfonamide Inhibitor Acetazolamide (AAZ) by a Stopped Flow CO_2 Hydrase Assay

	K_i (nM)[a]	
	hCA IX	hCA XII
2	653.7	727.5
10[b]	6830	4510
AAZ	25.2	5.7

[a]Mean from three different assays, by a stopped flow technique (errors were in the range of ±5−10% of the reported values). [b]Reference Supporting Information, Figure S7. Inhibitor concentration ranged from 10^{-8} to 10^{-5} M (see also Supporting Information, Figure S3)

response curves). From the data shown in Table 2, **2** clearly arose as a good *h*CA IX and *h*CA XII inhibitor, with K_i ranging in high nanomolar range (respectively 653.7 and 727.5 nM). Such results ascribed to **2** are lower in efficacy than the clinically used AAZ but improved compared to derivative **10**. Anyhow, it should be stressed that the sulfonate derivative **10** originates from the CA-mediated hydrolysis of the corresponding sulfocoumarin necessary to generate the active species from the original prodrug.[10] Conversely, such activation was not necessary in the case of **2**, which can directly bind the active site pocket.

Molecular Modeling. To fully explore the binding interaction of the sulfonate derivative **2** within CA active site, we undertook docking studies by taking into consideration the tumor-associated isoform *h*CA IX. In fact, all the attempts to co-crystallize **2** with CA failed, and at present, only one X-ray structure of a sulfonate compound within CA is available in Protein Data Bank, that is, the adduct of derivative **10** with a modified *h*CA II (PDB 4BCW).[10] This structure, also referred as *h*CA II/IX mimic, concerns an engineered protein in which two amino acid mutations are present in the *h*CA II active site, namely A65S and N67Q, serine and glutamine being the corresponding amino acids found in *h*CA IX. The sulfonate group of **10**, which as previously mentioned comes from the CA-mediated hydrolysis of the corresponding sulfocoumarin,[10] was found to anchor to the Zn-coordinated water molecule, differently from compounds containing the sulfonamide moiety that instead directly coordinates to the Zn ion.[20] Considering that **2** was assayed in vitro against *h*CA IX (K_i = 653.7 nM), the target used in such experiments was prepared by superposing 3IAI (*h*CA IX) and 4BCW (*h*CA II/IX mimic) through the Zn ion and the backbone of H94, H96, and H119 residues, then joining together only the enzyme 3D coordinates of 3IAI and the catalytic Zn coordinated OH/H_2O group of 4BCW. We report herein only the results obtained for the isomer R, as the stereocenter is located at the outer rim of the aliphatic tail of the molecule and barely affects the poses arising from the docking studies, thus the highlighted binding mode. Taking as the driving principle in the selection of the docking solutions the position of the sulfonate group in the X-ray solved structure, three rather iso-energetic poses were selected, all characterized by low values of the scoring function (Figures 4 and 5).

In the three different poses, the sulfonate group was always found to be involved in a wide network of H-bonds (Figure

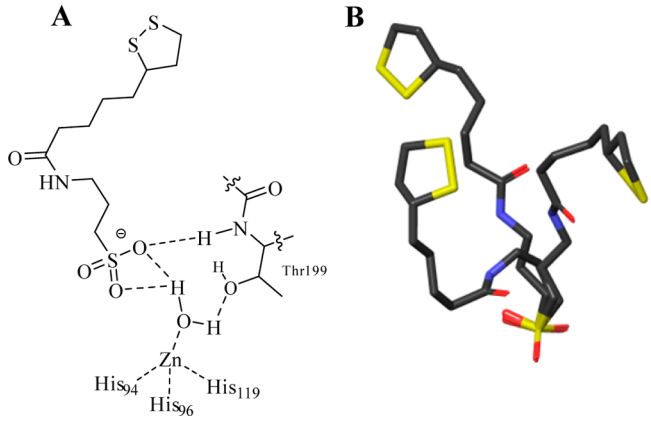

Figure 4. (A) Diagram of the H-bond network the sulfonate moiety is involved in within the active site cavity. (B) Superimposition of the three orientations found for **2** within *h*CA IX active site.

4A). In particular, two oxygen atoms of the sulfonate moiety accepted a H-bond from the Zn-bound water molecule, which in turn donates an additional one to OG1 oxygen of T199 side chain. Furthermore, one of these sulfonate O atoms established a H-bond with the backbone NH of T199, whereas the other one might be considered as "half-coordinated" to the Zn ion. The three **2** poses are differentiated by the position of the lipoic tail within the binding site cavity (Figure 4B), and each is characterized by hydrophobic contacts involving the propylenic linker and the lipoic moiety which respectively interact with L198, P201, and P202 (Figure 5A), V121, L91, V131, and Q92 (Figure 5B), and V121, W5, H64, and N62 (Figure 5C). Moreover, the amidic carbonyl of the conformers in Figure 5B,C is at H bond distance with Q92.

Compound 2 Reduces CA IX-Mediated Acidosis. Recently, to analyze the role of CA IX in cancer cells' motility, we investigated the extracellular pH in normoxia in extracted human prostate fibroblasts (HPFs) from healthy individuals affected by prostate hyperplasia, cancer-associated fibroblasts (CAFs), and in prostate cancer (PCa) cells after the treatment with conditioned medium (CM) from HPFs or CAFs.[21] The contact of CAFs with PCa cells gives rise to an increase in extracellular acidity ascribed to CA IX and suggesting that the conditioning loop among stromal and cancer cells involved in cancer cells malignancy and aggressiveness also takes into account acidification of the tumor microenvironment. In Figure 6, we report on the effect of **2** on alkalinization of extracellular pH in HPFs and CAFs. Fibroblasts were grown to subconfluence and serum starved for 48 h in the presence of **2** (100 μM); at the end of incubation, the pH of culture medium was immediately measured by a pH meter. We observed that the administration of **2** unambiguously reduces extracellular acidification, confirming a key role of CA IX in this phenomenon.

Compound 2 Positively Interferes in the Epithelial–Mesenchymal Transition (EMT) and Invasiveness in PCa Cells. A specific role is played by CA IX in the regulation of EMT of cancer cells, a key epigenetic program associated with increased motility, survival, and stemness.[21] In particular, we demonstrated that PCa cells undergo EMT in response to their contact with stromal fibroblasts expressing CA IX.[21] Here, we report on the effect of **2** on CAF-mediated EMT. PCa cells were treated for 72 h with conditioned medium (CM) obtained from HPFs and CAFs in the presence or not of **2** (100 μM).

DOI: 10.1021/acs.jmedchem.7b01237
J. Med. Chem. 2017, 60, 9003−9011

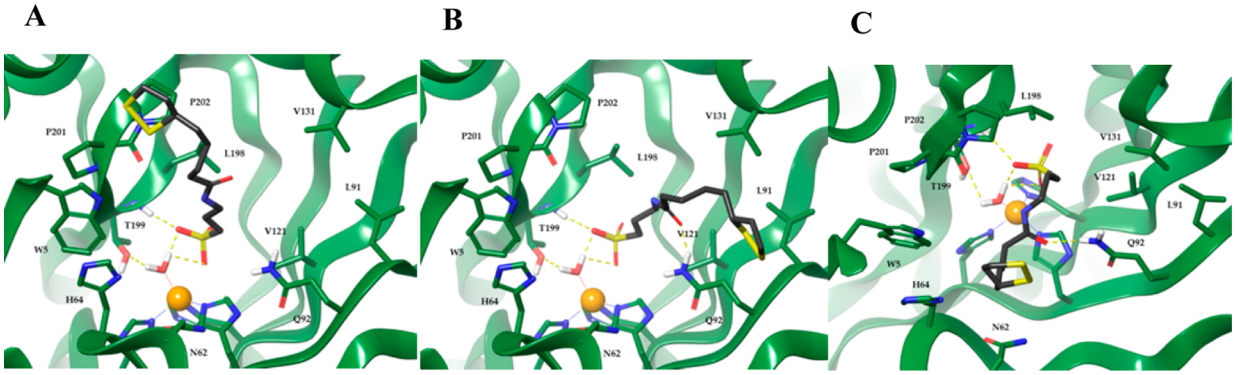

Figure 5. Simulated binding modes of compound **2** within *h*CA IX active site (PDB 3IAI): three diverse orientations are shown in panels A–C. The hydrogen bonds are shown as yellow dashed lines.

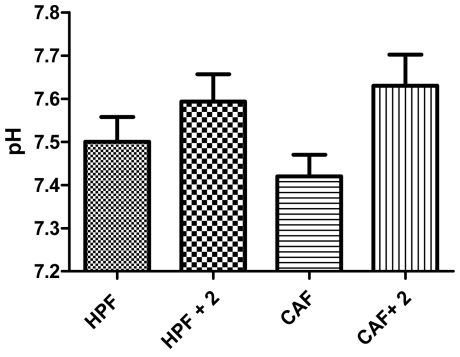

Figure 6. Effect of **2** on alkalinization of extracellular pH in HPF and CAF. Cells were serum starved and treated with 100 μM of **2** for 48h. *$p < 0.05$ vs CAF.

We observed that the use of the compound is active in impairing EMT in cancer cells due to CAFs contact (Figure 7A), preventing the elongation of the cells, as well as the expression of known EMT markers, as E-cadherin decrease and upregulation of Vimentin (Figure 7B).

In keeping rounded morphological features, **2** clearly affects invasiveness of cancer cells. We finally treated cells with CM from fibroblasts in the presence or not of **2** and assayed for their ability to invade through reconstituted matrigel barrier. Our data revealed that the ability of CAFs to elicit a pro-invasive behavior of cancer cells is severely impaired during the administration of **2** (Figure 8).

Compound 2 is a MMPs Inhibitor. As above-discussed, stromal CA IX leads to extracellular acidification. Because the sensitivity of MMPs to acidity is acknowledged and the key role played by CA IX in MMP-2 and MMP-9's secretion by CAFs is documented,[21] we reasoned that, given the similar active-site topology of MMPs and CAs, it would be worthy to investigate the binding properties of **2** vs MMPs. The intrinsic high similarity of human MMPs' active site, including MMP-2, MMP-9, and MMP-12, is well documented,[22,23] therefore, the catalytic domain of human MMP-12 has been used as a representative model of the whole protein family to analyze the

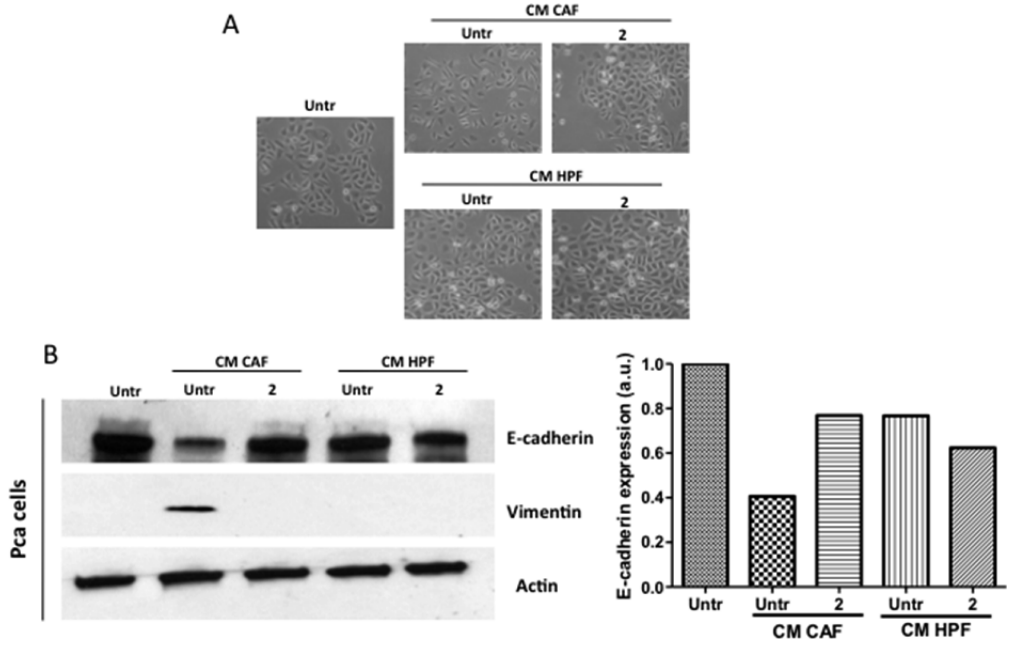

Figure 7. (A) HPF and CAF were treated with 100 μM of **2** for 48 h and CM were harvested. PCa cells were then treated with serum free medium or different CM for 72 h and then were photographed (B) Left: evaluation of E-cadherin and Vimentin in the same experimental setting described in A. (B) Right: actin immunoblot was used for normalization. Cadherin expression was shown in bar graph, a.u. = arbitrary units.

DOI: 10.1021/acs.jmedchem.7b01237
J. Med. Chem. 2017, 60, 9003–9011

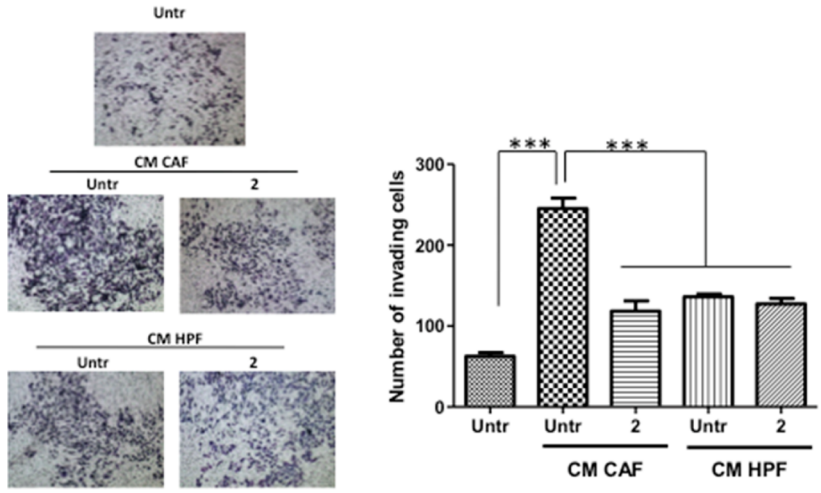

Figure 8. Left: invasion analysis of Pca cells after treatment for 24 h with different CM obtained from HPF or CAF (control or in the presence of **2**, 100 μM). Right: bar graph represents the mean of invading cells. *** <0.001 vs untreated CAF.

structural basis for the interaction of MMPs with the investigated scaffold. To determine the binding affinity of **2** for the catalytic domain of MMP-12, we analyzed the alteration of the chemical shifts observed in 2D $^{1}H-^{15}N$ HSQC spectra of the protein upon the titration with the lipoic acid derivative. Several residues forming the S1′ cavity and two zinc binding histidines experience a sizable chemical shift variation at submillimolar concentration of the ligand (see Figure 9). The fit of the experimental data provided a dissociation constant of 875 ± 78 μM.[24]

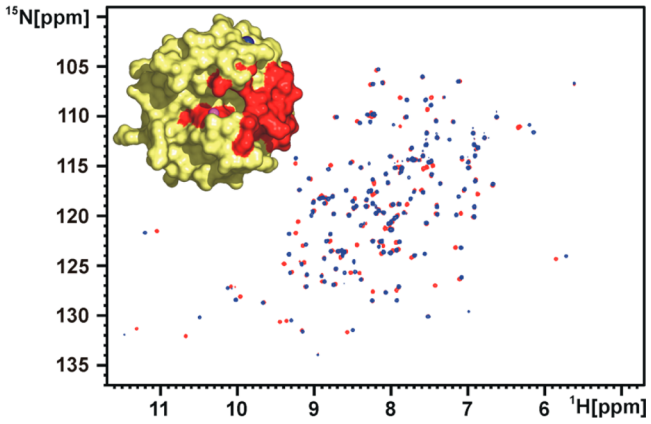

Figure 9. $^{1}H-^{15}N$ HSQC spectrum of the catalytic domain of MMP-12 in the absence (red) and presence of **2** (3.3 mM) (blue), with the surface model of MMP-12 showing in red the residues experiencing the largest chemical shifts variation.

The uncommon structure of **2** as MMP inhibitor deserved a more accurate investigation. Thus, a detailed structural characterization of the complex MMP-12-**2** by X-ray diffraction was carried out to investigate the binding mode and the involvement of the catalytic zinc in ligand binding. To confirm the structural data obtained, compound **9** (see Scheme 1) was synthesized and X-ray diffraction of the complex MMP-12−**9** performed. Compound **9** preserves the lipoic portion but presents a propyl alcohol replacing the propyl sulfonate residue of **2** (see Scheme 1).

Compound 2 and 9 Are Non-Zinc Binding Ligands of MMP-12. In both structures, AHA (hydroxamic acid, see Supporting Information) is not displaced by **2** or **9** and shows its typical binding to the catalytic zinc at full occupancy:[25] it chelates zinc with the two oxygens and establishes hydrogen bond interactions with the carbonyl amide oxygen of A182 and with a carboxylate oxygen of the catalytic E219. As consequence, the two lipoic-containing ligands do not interact directly with the catalytic zinc ion. As a matter of fact, the sulfonate residue (**2**) points outside the MMP-12's site and is placed at the very entrance of the substrate groove, in addition, one of the sulfonate oxygens is at 3.1 Å distant from the NH moiety of Y240. A second sulfonate oxygen is 2.7 Å far from the amidic carbonyl oxygen of G179. (Figure 10).

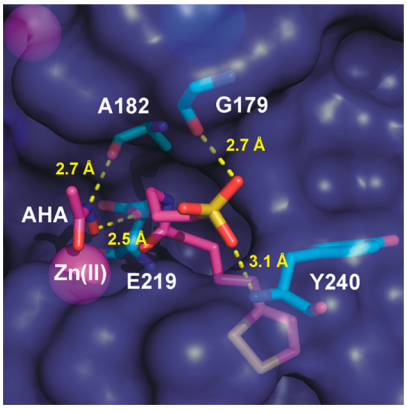

Figure 10. AHA and **2** placed into MMP-12 site. Hydrogen binding interactions are indicated as yellow dotted lines.

Likewise, the hydroxyl group of ligand **9** is located in the proximity of the groove entrance and it does not interact with any protein residue (Figure S6, Supporting Information). Both ligands bend similarly upon binding to the protein in such a way that the heterocyclic portion is accommodated into the S1′ pocket (Figure 11), while the chain occupies the groove normally occupied by the substrate before being hydrolyzed. The electron density of the lipoic-containing ligands appears of good quality in both cases, supporting their full occupancy; in detail, it shows that the heterocyclic ring of both **2** and **7**, containing a disulfide bridge, remains closed, witnessing that the S−S function is not reduced. In the case of the sulfonate

DOI: 10.1021/acs.jmedchem.7b01237
J. Med. Chem. 2017, 60, 9003−9011

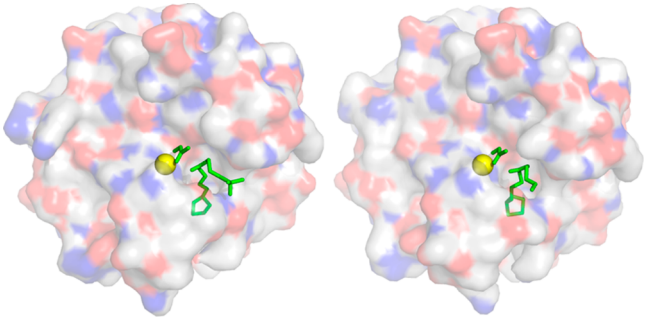

Figure 11. View of the interaction of **2** (left, PDB 5N5J) and **9** (right, PDB code 5N5K) with MMP-12. The two ligands and AHA are represented as green sticks, the protein as transparent surface, and the catalytic zinc as yellow sphere.

ligand, **2**, the two sulfur atoms of the ring into the S1′ pocket are placed at 3.6 Å from the carbonyl amide oxygens of V235 and F237. In the case of the OH ligand (compound **9**), the ring is slightly tilted so that the two sulfur atoms are at 3.6 Å from the carbonyl oxygens of T239 and K241. Moreover, the carbonyl amide oxygen present in the middle of the ligands points toward AHA, whereas the hydroxyl group of **9** and the sulfonate of **2** protrude outside the molecule toward the solvent (Figure 11).

DISCUSSION AND CONCLUSION

So far, OXA is the cancer drug commonly used to treat colorectal and resistant prostate cancer. However, the oxidative stress triggered by OXA induces a neuropathy, which is considered the neuropathic pain the most difficult to treat. In this article, we showed the properties of **2** to revert OXAIN in an experimental animal model, and we proved **2** effective in reducing cancer cells invasiveness by inhibiting CA IX in vitro. Compound **2**, formed by a lipoic acid residue linked to the homotaurine, has a remarkable safe profile in terms of cells viability and cardiotoxicity.[9] To exclude a possible effect of the distance between the cyclic disulfide and the sulfonic acid tail on the biological properties of **2**, the lower homologue **3** and the higher homologue **4** were synthesized. The lipoic portion of **2** reasonably accounts for the antioxidative properties we assessed in vitro (NBT test, Table S2, Supporting Information, and astrocytes cell culture Figure 2). In vivo, **2**, administered to rat previously treated with OXA, completely counteracted the OXA-induced hypersensitivity (see Figure 2B). The oxidative stress caused by OXA is also known to trigger the activation of the TRPA1 channel, evoking a noxious stimulus;[7] we confirmed **2** as an efficient inhibitor of TRPA1,[9] able to completely revert the OXA-induced activation of the channel (Figure 3). Compound **2** and the two homologues, namely **3** and **4**, showed similar antioxidative properties, close effects as TRPA1 inhibitors as well as in in vivo tests. This allows exclusion of any effect due to the distance between the disulfide bridge and the sulfonic acid portion.

The functional contribution of CA IX to specific biological processes critical for cancer progression, including pH regulation, migration, and invasion, provide the rational for its use as relevant therapeutic target.[18] In 2015, it was published the first example of CA IX inhibitor characterized by a sulfonate residue (see compound **10**, Figure 1). Considering the structural features of **2**, we investigated its binding affinity vs CA IX and CA XII, both involved in cancer progression. Tests of inhibition vs *h*CA IX and *h*CA XII clearly showed a high nanomolar affinity of **2** for both the CAs (Table 1). The binding interactions of the sulfonate **2** with the CA active site, explored while running computational studies, allowed us to properly rationalize the good inhibition constants assessed. We confirmed these inhibition properties by testing **2** in CA IX-mediated biochemical processes. We observed that the administration of **2** reduces extracellular acidification and clearly impairs EMT in cancer cells (Figure 7), preventing the expression of ETM markers and reducing invasiveness of cancer cells (Figure 8). These results were boosted by the synergist effect observed for **2** and OXA when used to treat HT-29 cancer cells (Table 1). These preliminary data suggest that the use of OXA and **2** in combination might allow decreasing of OXA concentration in therapy, reducing the painful effects produced. The binding properties of **2** vs MMPs were also examined. The chemical shifts recorded by 2D $^{1}H-^{15}N$ HSQC spectra of MMP-12 (model for the MMPs family, including the acidity sensitive MMP-2 and MMP-9) upon the titration with **2** provided a high micro molar K_d value. X-ray diffraction, carried out to investigate the binding mode of **2**, showed that it is a non-zinc binding ligand of MMP-12. Concluding, the simple structure of **2** collects unique biological properties: (i) it blocks OXA-induced TRPA1 current, (ii) reverts in vivo OXAIN, (iii) has a synergistic effect with OXA, (iv) inhibits CA IX and CA XII, two CAs involved in tumor progression, and (v) impairs EMT and invasiveness in cancer cells. Even though the inhibition of CAs should be confirmed in vivo, the unique properties of **2** and the soundness of the data reported could represent a glimmer in the dark scenario exposed to cancer patients suffering from the side effects related to the chronic administration of chemotherapy and from the intractable neuropathic pain induced by chemotherapy.

EXPERIMENTAL SECTION

Materials and Methods. Patch-clamp studies were carried out in Chinese hamster ovary (CHO) cells transiently expressing TRPA1 channel. For heterologous protein expression, cells were plated in 6-well cell culture dishes with 2 mL of growth medium, 24 h before transfection. Cells were transiently transfected using X-tremeGENE 9 transfection reagent (Roche) according to the protocol supplied by the manufacturer. EGFP fluorescence was used as marker of successful transfection. Electrophysiology studies were performed 48−72 h after transfection. Purity (≥95%) of compounds **3**, **4**, and **9** was determined by HRMS.

Male Sprague−Dawley (SD) rats (Harlan, Varese, Italy) weighing approximately 200−250 g at the beginning of the experimental procedure were used. Pirc (F344/NTac-Apc^{am1137}) rats, originally obtained from Taconic (Taconic Farms, Inc. USA), were bred in CESAL (Centro Stabulazione Animali da Laboratorio, University of Florence, Italy) in accordance with the Commission for Animal Experimentation of the Italian Ministry of Health. Animals were housed in CeSAL and used at least 1 week after their arrival.

2-(5-(1,2-Dithiolan-3-yl)pentammidoethanesulfonic Acid (3) and 4-(5-(1,2-Dithiolan-3-yl)pentamido)butane-1-sulfonic Acid (4): General Procedure. The activated lipoic acid **5** in DMF/H_2O as solvent was treated at room temperature with the aminosulfonic derivative **6**[26] or **7** to afford after purification by column chromatography on silica gel the derivatives **3** (60%) or **4** (80%), respectively, obtained as sodium salt. Compound **3**: Column chromatography on silica gel (eluent: CH_2Cl_2/MeOH 4/1; 5/2); glassy solid. ^{1}H NMR (500 MHz, D_2O): δ 3.67−3.62 (m, 1H, C*H*-3), 3.53−3.50 (t, $^{3}J_{(H,H)}$ = 6.8 Hz, 2H, CH_2-10), 3.22−3.12 (m, 2H, CH_2-1), 3.06−3.02 (t, $^{3}J_{(H,H)}$ = 6.8 Hz, 2H, CH_2-9), 2.46−2.41 (m, 1H, C*H*-2′), 2.23−2.20 (m, 2H, CH_2-7), 1.95−1.91 (m, 1H, C*H*-2), 1.73−1.56 (m, 3H), 1.40−1.36 ppm (m, 3H). ^{13}C NMR (125 MHz, D_2O): δ

DOI: 10.1021/acs.jmedchem.7b01237
J. Med. Chem. 2017, 60, 9003−9011

176.8, 56.5, 49.8, 40.3, 38.1, 35.5, 35.0, 33.7, 27.9, 24.9 ppm. HRMS calculated for $C_{10}H_{18}NO_4S_3^-$ $[M - H]^-$: 312.03980. Found: 312.03923. Elemental Anal. ($C_{10}H_{18}NNaO_4S_3$) Calculated: C, 35.81; H, 5.41; N, 4.18. Found: C, 35.78; H, 5.54; N, 4.46. Compound **4**: Column chromatography on silica gel (eluent: CH_2Cl_2/MeOH 4/1; 5/2); glassy solid. ^{1}H NMR (500 MHz, D_2O): δ 3.68−3.63 (m, 1H, C*H*-3), 3.20−3.12 (m, 4H, CH_2-1, CH_2-12), 2.88−2.85 (m, 2H, CH_2-9), 2.46−2.42 (m, 1H, C*H*-2), 2.21−2.18 (m, 2H, CH_2-7), 1.96−1.92 (m, 1H, C*H*-2′), 1.72−1.67 (m, 3H), 1.59−1.57 (m, 5H), 1.40−1.35 (m, 2H). ^{13}C NMR (125 MHz, D_2O): δ 176.8, 56.5, 50.6, 40.3, 38.8, 38.1, 35.6, 33.7, 27.8, 27.4, 25.1, 21.6 ppm. HRMS calculated for $C_{12}H_{22}NO_4S_3^-$ $[M - H]^-$: 340.07110. Found: 340.07008. Elemental Anal. ($C_{12}H_{22}NNaO_4S_3$) Calculated: C, 39.65; H, 6.10; N, 3.85. Found: C, 39.58; H, 6.32; N, 4.05.

5-(1,2-Dithiolan-3-yl)-*N*-(3-hydroxypropyl)pentanamide (9). A solution of the amino alcohol **8** (390 mg, 5.19 mmol) in DMF/H_2O was treated at room temperature with solid $NaHCO_3$ (5.19 mmol) then cooled to 0 °C. A solution of **5** (1.5 g, 4.94 mmol) in DMF was added and the reaction mixture warmed to room temperature and stirred overnight. Water (100 mL) was then added to the mixture and the organic layer extracted with EtOAc (2×). The crude (1.4 g) was purified by column chromatography on silica gel (eluent MeOH/DCM-8/1) to afford **9** as waxy solid (770 mg, 60%). Column chromatography on silica gel (eluent: CH_2Cl_2 with 8% MeOH); waxy solid. ^{1}H NMR (500 MHz, $CDCl_3$): δ 6.30 (bs, 1H, N*H*), 3.64−3.61 (m, 2H, CH_2-11), 3.59−3.54 (m, 1H, C*H*-3), 3.41−3.38 (m, 2H, CH_2-9), 3.27 (bs, 1H, O*H*), 3.20−3.09 (m, 2H, CH_2-1), 2.49−2.43 (m, 1H, C*H*-2), 2.24−2.18 (m, 2H, CH_2-7), 1.49−1.87 (m, 1H, C*H*-2′), 1.75−1.60 (m, 6H), 1.52−1.42 ppm (m, 2H). ^{13}C NMR (125 MHz, $CDCl_3$): δ 174.1, 59.4, 56.4, 40.3, 38.5, 36.4, 36.4, 34.6, 32.2, 28.9, 25.5 ppm. HRMS cald for $C_{11}H_{22}NO_2S_2^+$ $[M + H]^+$ 264.10920, found 264.10903. Elemental Anal. ($C_{11}H_{21}NO_2S_2$) Calculated: C, 50.16; H, 8.04; N, 5.32. Found: C, 50.08; H, 8.30; N, 5.02.

■ ASSOCIATED CONTENT

Supporting Information

The Supporting Information is available free of charge on the ACS Publications website at DOI: 10.1021/acs.jmedchem.7b01237.

^{1}H and ^{13}C spectra for compounds **3**, **4**, and **8**, in vitro and in vivo methods, *h*CAs inhibition, NMR spectroscopy, X-ray data (PDF)

Molecular formula strings (CSV)

Accession Codes

Authors will release the atomic coordinates and experimental data upon article publication. PDB codes: 5N5J for **2** and 5N5K for **9**.

■ AUTHOR INFORMATION

Corresponding Authors

*For C.N.: phone, (+39)0554573540; e-mail, cristina.nativi@unifi.it.

*For C.T.S.: e-mail, claudiu.supuran@unifi.it.

ORCID

Marco Fragai: 0000-0002-8440-1690

Alexandra Louka: 0000-0001-5054-6480

Barbara Richichi: 0000-0001-7093-9513

Paola Gratteri: 0000-0002-9137-2509

Francesco Tadini-Buoninsegni: 0000-0001-5594-2554

Claudiu T. Supuran: 0000-0003-4262-0323

Cristina Nativi: 0000-0002-6312-3230

Notes

The authors declare no competing financial interest.

■ ACKNOWLEDGMENTS

We are grateful to Prof. Claudio Luchinat (University of Florence) and Dr. Stefano Roelens (INSTM, Florence) for useful discussions. We thank Prof. Doug Golenbock (University of Massachusetts Medical School, Boston, USA) for providing pcDNA3-EGFP (Addgene plasmid no. 13031). Funding from Fondazione CRF no. 2014.0163, Banca CR Firenze 2016, and Istituto Toscano Tumori, ITT15.

■ ABBREVIATIONS USED

AAZ, acetazolamide; AHA, hydroxamic acid; CA, carbonic anhydrase; CAF, cancer associated fibroblasts; CIN, chemotherapy-induced neuropathy; CM, conditioned medium; EMT, epithelial−mesenchymal transition; MMP, matrix metalloproteinase; NBT, nitro blue tetrazolium; NHS, *N*-hydroxysuccinimide; OXA, oxaliplatin; OXAIN, OXA-induced neuropathic pain; SOD, superoxide dismutase; TRP, transient receptors potential

■ REFERENCES

(1) Woolf, C. J.; Mannion, R. J. Neuropathic pain: aetiology, symptoms, mechanisms and management. *Lancet* **1999**, *353*, 1959−1964.

(2) Majithia, N.; Loprinzi, C. L.; Smith, T. J. New practical approaches to chemotherapy-induced neuropathic pain: prevention, assessment and treatment. *Oncology (Williston Park)* **2016**, *30*, 1020−1029.

(3) Grothey, A. Clinical management of oxaliplatin-associated neurotoxicity. *Clin. Colorectal Cancer* **2005**, *5*, S38−S46.

(4) Hoshino, H.; Hida, K.; Ganeko, R.; Sakai, Y. Goshajinkigan for reducing chemotherapy induced peripheral neuropathy: protocol for a systematic review and meta-analysis. *Int. J. Colorectal Dis.* **2017**, *32*, 737−740.

(5) Argyriou, A. A.; Bruna, J.; Marmiroli, P.; Cavaletti, G. Chemotherapy-induced peripheral neuropathy: an update. *Crit. Rev. Oncol. Hematol.* **2012**, *82*, 51−77.

(6) Zhao, M.; Isami, K.; Nakamura, S.; Shirakawa, H.; Nakagawa, T.; Kaneko, S. Acute cold hypersensitivity characteristically induced by oxaliplatin is caused by the enhanced responsiveness of TRPA1 in mice. *Mol. Pain* **2012**, *8*, 55.

(7) Nassini, R.; Gees, M.; Harrison, S.; De Siena, G.; Materazzi, S.; Moretto, N.; Failli, P.; Preti, D.; Marchetti, N.; Cavazzini, A.; Mancini, F.; Pedretti, P.; Nilius, B.; Patacchini, R.; Geppetti, P. Oxaliplatin elicits mechanical and cold allodynia in rodends via TRPA1 receptors stimulation. *Pain* **2011**, *152*, 1621−1631.

(8) Nativi, C.; Gualdani, R.; Dragoni, E.; Di Cesare Mannelli, L.; Sostegni, S.; Norcini, M.; Gabrielli, G.; la Marca, G.; Richichi, B.; Francesconi, O.; Moncelli, M. R.; Ghelardini, C.; Roelens, S. A TRPA1 antagonist reverts oxaliplatin-induced neuropathic pain. *Sci. Rep.* **2013**, *3*, 2005.

(9) Gualdani, R.; Ceruti, S.; Magni, G.; Merli, D.; Di Cesare Mannelli, L.; Francesconi, O.; Richichi, B.; la Marca, G.; Ghelardini, C.; Moncelli, M. R.; Nativi, C. Lipoic-based TRPA1/TRPV1 antagonist to treat orofacial pain. *ACS Chem. Neurosci.* **2015**, *6*, 380−385.

(10) Grandane, A.; Tanc, M.; Di Cesare Mannelli, L.; Carta, F.; Ghelardini, C.; Zalubovskis, R.; Supuran, C. 6-Substituted sulfocumarins are selective carbonic anhydrase IX and XII inhibitors with significant cytotoxicity against colorectal cancer cells. *J. Med. Chem.* **2015**, *58*, 3975−3983.

(11) Gauchan, P.; Andoh, T.; Kato, A.; Kuraishi, Y. Involvement of increased expression of transient receptor potential melastin 8 in oxaliplatin-induced cold allodynia in mice. *Neurosci. Lett.* **2009**, *458*, 93−95.

(12) Descoeur, J.; Pereira, V.; Pizzoccaro, A.; Francois, A.; Ling, B.; Maffre, V.; Couette, B.; Busserolles, J.; Courteix, C.; Noel, J.;

DOI: 10.1021/acs.jmedchem.7b01237
J. Med. Chem. 2017, 60, 9003−9011

Lazdunski, M.; Eschalier, A.; Authier, N.; Bourinet, E. Oxaliplatin-induced cold hypersensivity is due to remodeling of ion channel expression in nociceptors. *EMBO Mol. Med.* **2011**, *3*, 266−178.
(13) Di Cesare Mannelli, L.; Pacini, A.; Bonaccini, L.; Zanardelli, M.; Mello, T.; Ghelardini, C. Morphologic features and glial activation in rat oxaliplatin-dependent neuropathic pain. *J. Pain* **2013**, *14*, 1585−1600.
(14) Di Cesare Mannelli, L.; Pacini, A.; Micheli, L.; Tani, A.; Zanardelli, M.; Ghelardini, C. Glial role in oxaliplatin-induced neuropathic pain. *Exp. Neurol.* **2014**, *261*, 22−33.
(15) Supuran, C. T. Carbonic Anhydrase: novel therapeutic applications for inhibitors and activators. *Nat. Rev. Drug Discovery* **2008**, *7*, 168−181.
(16) Neri, D.; Supuran, C. T. Interfering with pH regulation in tumor as a therapeutic strategy. *Nat. Rev. Drug Discovery* **2011**, *10*, 767−777.
(17) Swietach, P.; Hulikova, A.; Vaughan-Jones, R. D.; Harris, A. L. New insight into the physiological role of carbonic anhydrase IX in tumor pH regulation. *Oncogene* **2010**, *29*, 6509−6521.
(18) Tafreshi, N. K.; Lloyd, M. C.; Bui, M. M.; Gillies, R. J.; Morse, D. L. Carbonic anhydrase IX as an imaging and therapeutic target for tumors and metastases. *Subcell. Biochem.* **2014**, *75*, 221−254.
(19) Pacchiano, F.; Carta, F.; McDonald, P. C.; Lou, Y.; Vullo, D.; Scozzafava, A.; Dedhar, S.; Supuran, C. T. Ureido-substituted benzenesulfonamides potently inhibit carbonic anhydrase IX and show antimetastatic activity in a model of breast cancer metastasis. *J. Med. Chem.* **2011**, *54*, 1896−1902.
(20) Alterio, V.; Hilvo, M.; Di Fiore, A.; Supuran, C. T.; Pan, P.; Parkkila, S.; Scaloni, A.; Pastorek, J.; Pastorekova, S.; Pedone, C.; Scozzafava, A.; Monti, S. M.; De Simone, G. Crystal structure of the catalytic domain of the tumor-associated human carbonic anhydrase IX. *Proc. Natl. Acad. Sci. U. S. A.* **2009**, *106*, 16233−16238.
(21) Fiaschi, T.; Giannoni, E.; Taddei, M. L.; Cirri, P.; Marini, A.; Pintus, G.; Nativi, C.; Richichi, B.; Scozzafava, A.; Carta, F.; Torre, E.; Supuran, C. T.; Chiarugi, P. Carbonic Anhydrase IX from cancer-associated fibriblastes drives epitelial-mesenchymal transition in prostate carcinoma cells. *Cell Cycle* **2013**, *12*, 1791−1801.
(22) Bertini, I.; Calderone, V.; Cosenza, M.; Fragai, M.; Lee, Y. M.; Luchinat, C.; Mangani, S.; Terni, B.; Turano, P. Conformational variability of matrix metalloproteinases: beyond a single 3D structure. *Proc. Natl. Acad. Sci. U. S. A.* **2005**, *102*, 5334−5339.
(23) Rao, B. G. Recent developments in the design of specific Matrix Metalloproteinase inhibitors aided by structural and computational studies. *Curr. Pharm. Des.* **2005**, *11*, 295−322.
(24) Winter, A.; Sigurdardottir, A. G.; Di Cara, D.; Valenti, G.; Blundell, T. L.; Gherardi, E. Developing antagonists for theMet/HGF/SF protein-protein interaction using a fragment-based approach. *Mol. Cancer Ther.* **2016**, *6*, 3−14.
(25) Udi, Y.; Fragai, M.; Grossman, M.; Mitternacht, S.; Arad-Yellin, R.; Calderone, V.; Melikian, M.; Toccafondi, M.; Berezovsky, I. N.; Luchinat, C.; Sagi, I. Unraveling hidden regulatory sites in structurally homologous metalloproteinases. *J. Mol. Biol.* **2013**, *425*, 2330−2346.
(26) Deng, H.; Liu, X.; Xie, J.; Yin, R.; Huang, N.; Gu, Y.; Zhao, J. Quantitative and site-directed chemical modification of hypocrellins toward direct drug delivery and effective photodynamic activity. *J. Med. Chem.* **2012**, *55*, 1910−1919.

DOI: 10.1021/acs.jmedchem.7b01237
J. Med. Chem. 2017, 60, 9003−9011